

Development of an Isomeric Beam of ^{26}Al for Nuclear Reaction Studies

B. W. Asher^a, S. Almaraz-Calderon^a, O. Nusair^b, K. E. Rehm^b, M. L. Avila^b, A. A. Chen^d, C. A. Dickerson^b, C. L. Jiang^b, B. P. Kay^b, R. C. Pardo^b, D. Santiago-Gonzalez^{c,b}, R. Talwar^b

^a*Department of Physics, Florida State University, Tallahassee, Florida 32306, USA*

^b*Physics Division, Argonne National Laboratory, Argonne, Illinois 60439, USA*

^c*Department of Physics and Astronomy, Louisiana State University, Baton Rouge, Louisiana 70803, USA*

^d*Department of Physics and Astronomy, McMaster University, Hamilton, Ontario L8S 4M1, Canada*

Abstract

This paper describes the production and characterization of a ^{26}Al beam comprised of both, its 5^+ ground state, and its 0^+ isomeric state. The ^{26}Al beam was produced in-flight via the $p(^{26}\text{Mg}, ^{26}\text{Al})n$ reaction. The isomer fraction of the ^{26}Al beam was maximized by choosing a bombarding energy of 158.5 MeV for the ^{26}Mg primary beam. The resulting beam had an energy of 120 MeV, a total intensity of 2×10^5 particles/sec, a purity of 98% and an isomer content of 70%. This high-quality ^{26}Al isomeric beam was used to study the $^{26}\text{Al}^m(d,p)^{27}\text{Al}$ reaction relevant for understanding the nucleosynthesis of ^{26}Al in the Galaxy.

1. Introduction

The detection of cosmic gamma-rays by space telescopes has become a very powerful tool for understanding the synthesis of elements in the Galaxy [1]. Of special interest is the detection of the 1809-keV gamma-ray line which has been observed by several gamma-ray space telescopes [2, 3], and is associated with the decay of the radioactive nucleus ^{26}Al . This gamma-ray is attributed to the β^+ -decay of the 5^+ ground state of ^{26}Al ($^{26}\text{Al}^g$, $t_{1/2} = 717,000$

yr) to the first excited 2^+ state in ^{26}Mg which then decays via the 1809-keV gamma-ray to the ground state of ^{26}Mg . Since the half-life of ^{26}Al is much shorter than the average age of the Galaxy, the detection of this gamma-ray line provides strong evidence for ongoing nucleosynthesis in the Galaxy [4]. Detailed maps of the distribution of the 1809-keV gamma-ray line provided by space telescopes suggest that massive stars are the main production sites of ^{26}Al in the Galaxy. In order to correctly interpret the observations and evaluate their impact, experiments in the laboratory need to

Email address: salmarazcalderon@fsu.edu (S. Almaraz-Calderon)

25 be performed to understand all the reactions
 26 that produce and destroy ^{26}Al in stellar en-
 27 vironments. The presence of a low-lying 0^+
 28 isomeric state in ^{26}Al ($^{26}\text{Al}^m$, $t_{1/2} = 6.35$ s)
 29 however, strongly complicates the calibration
 30 of its nucleosynthesis. The 0^+ isomeric state
 31 in ^{26}Al decays directly to the ground state of
 32 ^{26}Mg bypassing the emission of the 1809-keV
 33 gamma-ray. This is illustrated in the partial
 34 level scheme in Fig. 1 which shows the rele-
 35 vant states of ^{26}Al and ^{26}Mg . It has been sug-
 36 gested that radiative proton captures on both,
 37 the ground and the isomeric states, are the
 38 main destruction paths of ^{26}Al in asymptotic
 39 giant branch (AGB) stars, classical novae (CN)
 40 and core collapse supernovae (CCSN) [5]. Due
 41 to its astrophysical relevance, the production
 42 and use of an isomeric $^{26}\text{Al}^m$ (0^+) beam has
 43 been the goal at several laboratories around the
 44 world (e.g. TRIUMF, TAMU, RIBF-RIKEN,
 45 KVI Gronengen [6–9]).

46 In this paper, we report on the first pro-
 47 duction of an isomeric $^{26}\text{Al}^m$ beam with a
 48 high isomer content, intensity and purity. The
 49 $^{26}\text{Al}^m$ beam was then used for a measurement
 50 of the $^{26}\text{Al}(d,p)^{27}\text{Al}$ reaction, where states in
 51 ^{27}Al were populated via low angular momen-
 52 tum transfers from ^{26}Al . Our experimental
 53 measurement puts a limit on the nucleosynthe-
 54 sis rate of the $^{26}\text{Al}^m(p,\gamma)^{27}\text{Si}$ reaction which is

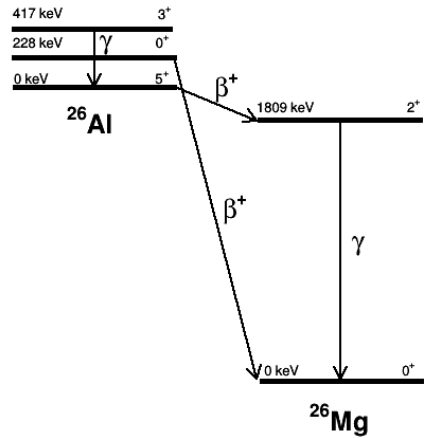


Figure 1: Partial level scheme of ^{26}Al and ^{26}Mg illustrating the β^+ transitions from $^{26}\text{Al}^m$ ($t_{1/2} = 6.35$ s) to the ground state of ^{26}Mg and of $^{26}\text{Al}^g$ ($t_{1/2} = 717000$ yr) to the 2^+ state of ^{26}Mg followed by the 1809-keV gamma-ray to the ground state of ^{26}Mg .

55 one of the main destruction paths of ^{26}Al in
 56 the Galaxy [10].

2. ^{26}Al Beam Production

58 The ^{26}Al beam was produced via the
 59 $^{26}\text{Mg}(p,n)^{26}\text{Al}$ reaction, in inverse kinematics,
 60 at the ATLAS in-flight facility at Argonne Na-
 61 tional Laboratory. Previous cross section mea-
 62 surements of the $^{26}\text{Mg}(p,n)^{26}\text{Al}$ reaction were
 63 fundamental for the beam production and en-
 64 hancement of the isomeric content of the beam
 65 [11, 12]. The excitation function as measured
 66 by Doukellis et al. [11] using a proton beam to
 67 bombard a ^{26}Mg target and to produce ^{26}Al ,
 68 is shown in Fig. 2. Neutrons from the 5^+ , 0^+ ,
 69 and 3^+ states in ^{26}Al populated via the (p,n)

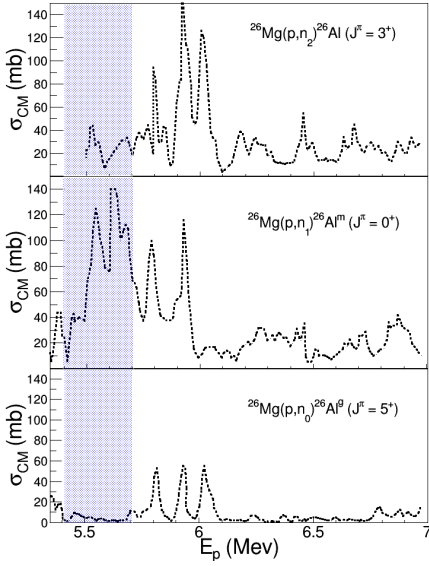


Figure 2: Cross section of the $^{26}\text{Mg}(\text{p},\text{n})^{26}\text{Al}$ reaction measured by Doukellis et al. [11]. The shaded region indicates the chosen energy range for the present experiment to maximize production of the isomer. Adapted from Ref. [11]

reaction were measured and their relative cross sections were extracted. As can be seen from the highlighted area in Fig. 2, a high percentage of the isomeric $^{26}\text{Al}^m$ beam can be obtained if the proton energy is chosen to be between $E_p = 5.4 - 5.7$ MeV. For an inverse kinematic reaction this corresponds to ^{26}Mg energies between $E_{lab} (^{26}\text{Mg}) = 140.3 - 148.1$ MeV.

A ^{26}Mg primary beam with an energy of 158.5 MeV was used to bombard a H_2 filled gas cell in order to produce ^{26}Al via the $p(^{26}\text{Mg}, ^{26}\text{Al})n$ reaction. The gas cell [13] was 3.7 cm long and enclosed by two HAVARTM windows of 1.9 mg/cm^2 thickness each, re-

sulting in an energy loss of 9.5 MeV of the ^{26}Mg beam before reaching the hydrogen gas at about 149 MeV. The gas was pressurized to 1000 Torr and kept at room temperature (293 K) achieving an effective target thickness of $0.41 \text{ mg}/\text{cm}^2$. Under these conditions, the primary beam loses about 8.5 MeV through the gas. This results in an energy of the ^{26}Mg primary beam in the range of 5.7 - 5.4 MeV/u at which it will interact with the hydrogen gas. The corresponding proton energy in normal kinematics is indicated by the shaded energy range shown in Fig. 2. A secondary 120 MeV beam of ^{26}Al was produced along with unreacted ^{26}Mg from the primary source material in their various charge states. The contaminants were filtered out primarily by a 22° bending magnet located downstream from the production gas cell [13]. A schematic of the beam production is shown in Fig. 3.

3. Beam Characterization

The profile of the beam was measured with a silicon detector located in the characterization station depicted in Fig. 3. To reduce the primary and thus the secondary beam intensities, a 1/1000 attenuator was inserted after the ion source to insure good working condition of the silicon detector used for characterization. After the 22° bending magnet shown in Fig.

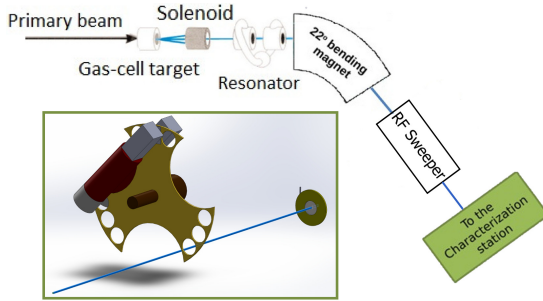


Figure 3: Schematics of the beam production setup. After the primary beam interacts with the gas cell, a solenoid, a 22° magnet, and an radio frequency (RF) sweeper are used to select, focus and reduce contaminants of the radioactive beam. The insert in the lower left part of the figure is a 3D-model of the characterization station composed of a rotating wheel, two NaI detectors, and a silicon detector which are described in Section 3. Adapted from Ref. [14].

113 3, the secondary beam still contains contam-
 114 inants with magnetic rigidities similar to the
 115 one of the ^{26}Al ($q = 13^+$) beam. These con-
 116 taminants were removed through the use of a 133
 117 radio frequency (RF) sweeper [15]. Optimiza- 134
 118 tion of the RF sweeper resulted in a 120 MeV 135
 119 ^{26}Al beam with about 98% purity and 1% en- 136
 120 ergy resolution (FWHM). The optimized beam 137
 121 as measured by the silicon detector placed in 138
 122 the characterization station with an attenu- 139
 123 ated primary beam is shown in Fig. 4, where 140
 124 the final contaminants are mainly lower charge 141
 125 states of the primary beam. From the count 142
 126 rate obtained in this measurement and the at- 143
 127 tenuation factor of 1/1000, the intensity of the 144
 128 total ^{26}Al beam (g.s. and isomer) was deter- 145

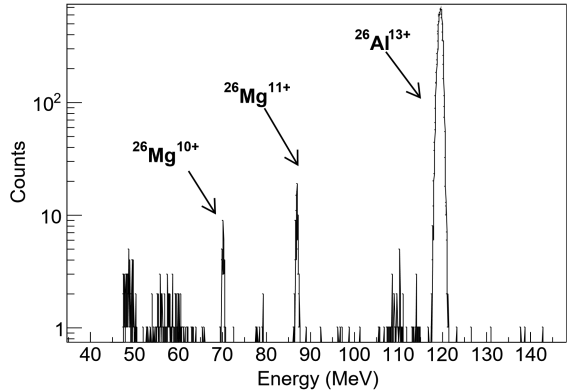


Figure 4: Beam profile after the magnetic rigidity was set for ^{26}Al ($q=13^+$) and the RF sweeper was optimized. The 12^+ charged state of the primary ^{26}Mg beam was completely removed. The remaining contaminants ($\leq 2\%$) are mainly lower charge states of ^{26}Mg .

129 mined, with a typical value of about 2×10^5 par-
 130 ticles/sec per 20-30 pnA of primary ^{26}Mg beam
 131 incident on the production target.

132 The isomeric content of the beam ($^{26}\text{Al}^m$)
 133 was measured through its β^+ -decay radia-
 134 tion, which was followed by positron-electron
 135 annihilation that resulted in two 511-keV
 136 gamma-rays. The measurement of the 511-keV
 137 gamma-ray was performed by using the rotat-
 138 ing wheel setup shown in Fig. 5 which was
 139 located about 50 cm upstream of the Si detec-
 140 tor. A 100 mg/cm² thick Au foil was mounted
 141 at the bottom of the rotating wheel as shown
 142 in Fig. 5(a). The Au foil was chosen because
 143 its high Z and therefore a high Coulomb barrier
 144 prevented nuclear reactions with the 120 MeV
 145 ^{26}Al beam. The Au foil was bombarded by

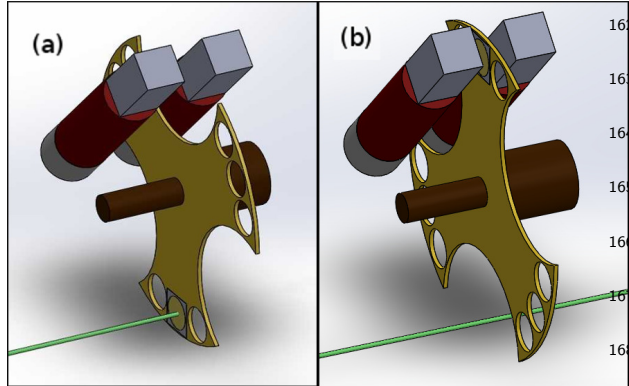


Figure 5: Schematics of the rotating wheel setup used to measure the isomer content of the beam. (a) A Au foil was irradiated by the beam for 15 s. (b) The Au foil was then rotated by 180° and placed in between two NaI detectors where the gamma-rays are measured for another 15 s.

the ^{26}Al beam for 15 seconds (~ 2 half-lives of $^{26}\text{Al}^m$). After this irradiation time, the Au foil was rotated by 180° to a position in between two NaI detectors, shown in Fig. 5(b) where a measurement of the 511-keV annihilation radiation was performed for another 15 seconds. A 48-bit latching scalar was added to the electronics to obtain the timing information from the events measured in the NaI detectors.

Fig. 6 shows a coincidence spectrum of the two NaI detectors. The $^{26}\text{Al}^g$ (5^+) g.s. also undergoes a β^+ -decay, but, since the half-life of the ground state is much longer ($t_{g,1/2} = 717,000$ years) than that of the isomeric state, the contribution of β^+ -decays from $^{26}\text{Al}^g$ in the time of the measurement is negligible. The tim-

ing of the 511-keV gamma-rays measured with the NaI detectors was extracted and a decay curve was fitted. Since the decay was taken in cycles lasting 15 second each, the intervals were later summed to improve the statistics. A typical summed run is shown in Fig. 7. The fit to the decay curve gives a half-life of 6.2 ± 0.2 seconds, in good agreement with the accepted half-life of 6.35 seconds of the $^{26}\text{Al}^m$ [16], confirming the existence and positive identification of the isomer. The detection efficiency of the NaI detectors for 511-keV photons was calculated using a GEANT4 simulation which was validated with a calibrated ^{22}Na source placed at the Au foil position. The measurement of the 511-keV photons from the source was compared with the counts from the simulation and were found to agree within 10%. For the configuration used in this experiment, the simulated single-photon efficiencies for 511-keV photons were found to be $1.82\% \pm 0.02\%$ and $1.90\% \pm 0.02\%$ for each NaI detector while for the coincidence efficiency a value of $0.07\% \pm 0.01\%$ was obtained [14]. The yield from the coincident 511-keV gamma radiation was then integrated, adjusted for efficiency as calculated by the GEANT4 simulation, and divided by the total ^{26}Al yield measured in the silicon detector. This resulted in a $70 \pm 10\%$ isomeric-to-ground-state ratio. This result is shown by the

192 solid point in Fig. 8.

193 The present experimental value extracted for
194 the isomeric-to-ground-state ratio is in good
195 agreement with the ratio extracted from the
196 cross section measurements by Doukellis et al.
197 [11] shown in Fig. 2 when the data is aver-
198 aged to take into account the extended geom-
199 etry and the energy loss of the production tar-
200 get. This agreement is shown in Fig. 8 where
201 the present experimental value is indicated by
202 the solid point and the solid line is obtained by
203 averaging the experimental data in Fig. 2 over
204 the energy loss of the ^{26}Mg beam in the pro-
205 duction target. It can also be noted that by in-
206 creasing the bombarding energy to 6.1 MeV/u
207 one can invert the isomer-to-ground-state ratio
208 to 0.2. Included also in Fig. 8 is the isomer-
209 to-ground state ratio that would be expected
210 if the energy loss in the gas target is reduced
211 from 325 keV to 100 keV (dashed line). As can
212 be seen in the figure, an increase in the ratio
213 to about 0.9 could be obtained by using a thin-
214 ner target with an incident energy of about 5.7
215 MeV/u. The higher isomeric ratio, however,
216 would come at the expense of a lower radioac-
217 tive beam intensity due to the lower effective
218 target thickness. At the moment, the main lim-
219 itation in the production of this isomeric beam
220 is the amount of primary beam that the win-
221 dows in the gas cell can tolerate without risk-

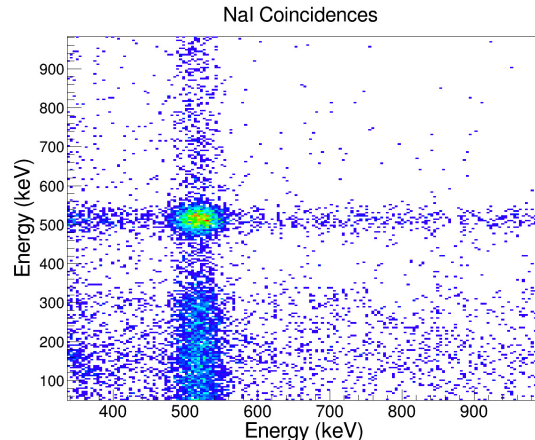


Figure 6: Energy spectra from the two NaI detectors used to measure the gamma radiation implanted in an Au foil plotted against each other. Here, the coincident 511-keV gamma-rays are clearly visible. A 48-bit latching scalar was 'latched' to the NaI detectors to get the timing information of the events. Gating on these coincidences allowed the measurement of the half-life of the decay radiation and confirm the presence of $^{26}\text{Al}^m$.

222 ing breakage (~ 20 - 30 pnA). Next genera-
223 tion hydrogen targets, e.g. using thin films of
224 hydrogen-containing oils [17] should be able to
225 tolerate higher primary beam intensities in or-
226 der to enhance the secondary beam yields.

227 4. Conclusions

An isomeric ^{26}Al (0^+) beam was success-
228 fully produced at the ATLAS accelerator facil-
229 ity at Argonne National Laboratory using the
230 in-flight production method with a ^{26}Mg beam
231 bombarding a hydrogen gas target. A silicon
232 detector, a rotating wheel, and NaI detectors
233 were used to characterize the beam. By choos-

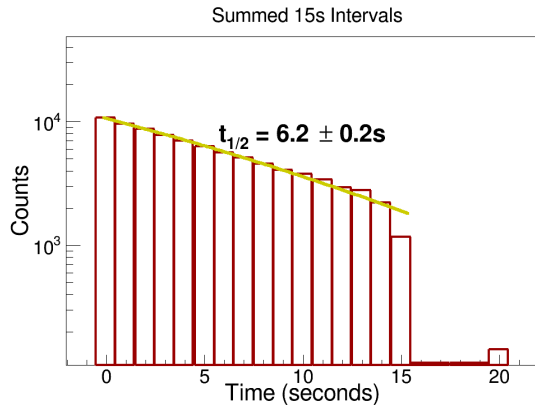


Figure 7: Timing spectrum associated with coincidences of 511-keV gamma radiation measured in the two NaI detectors summed over 15 second time intervals. The exponential decay fit yields a 6.2 ± 0.2 s half-life in agreement with the accepted 6.35 s half-life of $^{26}\text{Al}^m$.

235 ing the appropriate energy of the primary ^{26}Mg
 236 beam and the pressure and temperature of the
 237 production gas cell filled with H_2 , we have suc-
 238 cessfully produced a beam of $^{26}\text{Al}^m$ with 1%
 239 energy resolution, 98% purity, a total intensity 254
 240 of 2×10^5 particles/sec, and a 70% isomer con- 255
 241 tent.

242 This technique opened the possibility for us- 257
 243 ing isomeric beams as probes to explore re- 258
 244 actions that previously could not be studied, 259
 245 thus, making the technique a very powerful 260
 246 tool in nuclear reactions, nuclear structure and 261
 247 nuclear astrophysics studies. A study of the 262
 248 $^{26}\text{Al}^m(d,p)^{27}\text{Al}$ reaction which was the moti- 263
 249 vation for this development has already been 264
 250 performed [10]. Studies of similar reactions us- 265
 251 ing e.g. ^{34}Cl , ^{38}K [18], and ^{18}F [19] beams are 266

252 already ongoing or planned in the near future.

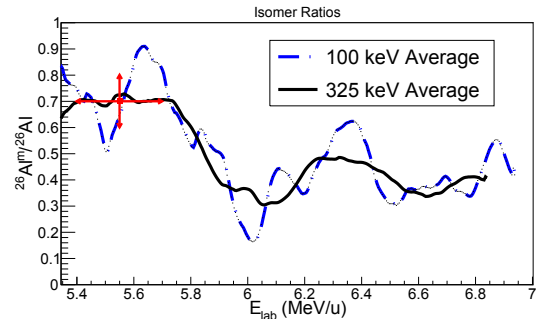


Figure 8: Ratio of isomer to ground state components of the ^{26}Al beam as function of the energy of the primary beam. The solid and dashed lines were extracted from the measurement of Ref. [11] by averaging the cross sections using the different effective target thicknesses indicated in the figure. The solid point is the value of the ratio measured in this experiment.

Acknowledgements

This work was partially supported by the State of Florida, the NSF under grant PHY-1712953 and the U.S. Department of Energy, Office of Nuclear Physics, under contract No. DE-AC02-06CH11357 (ANL). D.S.G. acknowledges the support by the U.S. Department of Energy, Office of Nuclear Physics, under grant No. DE-FG02-96ER40978. A.A.C. acknowledges support by the Natural Sciences and Engineering Research Council of Canada. This research used resources of ANL's ATLAS facility, which is a DOE Office of Science User Facility.

267 **5. References** 304

268 [1] Wang, W., Lang, M. G., Diehl, R., Halloin, H., 306
Jean, P., Knöldlseder, J., Kretschmer, K., Martin, 307
P., Roques, J. P., Strong, A. W., Winkler, C., 308
Zhang, X. L., [Spectral and intensity variations of](#) 309
galactic ^{26}Al emission, *Astron. Astrophys.* 496 (3) 310
(2009) 713–724. 311
URL <https://doi.org/10.1051/0004-6361/200811175> 312

273 [2] W. A. Mahoney, J. C. Ling, A. S. Jacobson, R. E. 314
Lingenfelter, Diffuse galactic gamma-ray line emis- 315
sion from nucleosynthetic Fe-60, Al-26, and Na-22 316
- Preliminary limits from HEAO 3, *Astrophysical* 317
Journal 262 (1982) 742. [doi:10.1086/160469](https://doi.org/10.1086/160469). 318

276 [3] R. Diehl, C. Dupraz, K. Bennett, H. Bloe- 319
men, W. Hermsen, J. Knoedlseder, G. Lichten, 320
D. Morris, J. Ryan, V. Schoenfelder, H. Steinle, 321
A. Strong, B. Swanenburg, M. Varendorff, C. Win- 322
kler, COMPTEL observations of Galactic ^{26}Al 323
emission., *Astron. Astrophys.* 298 (1995) 445. 324

281 [4] N. Prantzos, R. Diehl, [Radioactive \$^{26}\text{Al}\$ in the](#) 325
galaxy: observations versus theory, *Physics Re-* 326
ports 267 (1) (1996) 1 – 69. 327
URL <http://www.sciencedirect.com/science/article/pii/0370157395000550> 328

289 [5] C. Iliadis, A. Champagne, A. Chieffi, M. Limongi, 330
The effects of thermonuclear reaction rate varia- 331
tions on ^{26}Al production in massive stars: A sen- 332
sitivity study, *The Astrophysical Journal Supple-* 333
ment Series 193 (1) (2011) 16. 334
URL <http://stacks.iop.org/0067-0049/193/i=1/a=16> 335

299 [6] C. Ruiz, [Triumf proposal 989](#), 2005. 337
URL <http://dragon.triumf.ca/experiments/e989.pdf> 338

301 [7] B. Roeder, [Tamu cyclotron institute progress](#) 340
report (2011-2012), 2011-2012. 341

304 URL https://cyclotron.tamu.edu/progress-reports/2011-2012/cyclotron_progress_2012.pdf

305 [8] D. Kahl, Explosive destruction of ^{26}Al , *Il Nuovo*
Cimento [doi:10.1393/ncc/i2016-16362-2](https://doi.org/10.1393/ncc/i2016-16362-2).

311 [9] O. Grasdijk, Production of a beam of isomeric
 ^{26}Al for astrophysical research (2011).
URL https://www.astro.rug.nl/opleidingsinstituut/reports/bachelor/Phys_Bc_2011_JOGrasdijk.pdf

313 [10] S. Almaraz-Calderon, K. E. Rehm, N. Gerken,
M. L. Avila, B. P. Kay, R. Talwar, A. D.
Ayangeakaa, S. Bottoni, A. A. Chen, C. M.
Deibel, C. Dickerson, K. Hanselman, C. R. Hoff-
man, C. L. Jiang, S. A. Kuvin, O. Nusair, R. C.
Pardo, D. Santiago-Gonzalez, J. Sethi, C. Ugalde,
Study of the $^{26}\text{Al}^m(d, p)^{27}\text{Al}$ reaction and the
influence of the ^{26}Al 0^+ isomer on the destruction
of ^{26}Al in the galaxy, *Phys. Rev. Lett.* 119 (2017)
072701. [doi:10.1103/PhysRevLett.119.072701](https://doi.org/10.1103/PhysRevLett.119.072701).
URL <https://link.aps.org/doi/10.1103/PhysRevLett.119.072701>

318 [11] G. Doukellis, J. Rapaport, The $^{26}\text{Mg}(p, n)^{26}\text{Al}$ and
 $^{23}\text{Na}(\alpha, n)^{26}\text{Al}$ reactions near threshold, *Nuclear*
Physics A 467 (3) (1987) 511 – 527.
URL <http://www.sciencedirect.com/science/article/pii/0375947487905422>

327 [12] R. T. Skelton, R. W. Kavanagh, D. G. Sargood,
 $^{26}\text{Mg}(p, n)^{26}\text{Al}$ and $^{23}\text{Na}(\alpha, n)^{26}\text{Al}$ reactions, *Phys.*
Rev. C 35 (1987) 45–54.
URL <https://link.aps.org/doi/10.1103/PhysRevC.35.45>

336 [13] B. Harss, R. C. Pardo, K. E. Rehm, F. Borasi, J. P.
Greene, R. V. F. Janssens, C. L. Jiang, J. Nolen,
M. Paul, J. P. Schiffer, R. E. Segel, J. Specht, T. F.
Wang, P. Wilt, B. Zabransky, Production of ra-
dioactive ion beams using the in-flight technique,
Review of Scientific Instruments 71 (2) (2000) 380–

342 387.

343 URL <https://doi.org/10.1063/1.1150211>

344 [14] O. Nusair, Production of secondary radioactive ion
345 beam via few-nucleon transfer reactions. frankfurt
346 am main, Ph.D. thesis, Frankfurt am Main (2015).

347 [15] R. Pardo, J. Bogaty, S. Sharamentov, K. Rehm,
348 An rf beam sweeper for purifying in-flight pro-
349 duced secondary ion beams at atlas, Nuclear In-
350 struments and Methods in Physics Research Sec-
351 tion A: Accelerators, Spectrometers, Detectors and
352 Associated Equipment 790 (Supplement C) (2015)
353 1 – 5.

354 URL <http://www.sciencedirect.com/science/article/pii/S0168900215003630>

356 [16] M. Basunia, A. Hurst, Nuclear data sheets 134, 1
357 (2016) (2016).

358 [17] B. B. Back, J. A. Clark, R. C. Pardo, K. E. Rehm,
359 G. Savard, *Astrophysics experiments with radioac-*
360 *tive beams at atlas*, AIP Advances 4 (4) (2014)
361 041005.

362 URL <https://doi.org/10.1063/1.4865588>

363 [18] S. Almaraz-Calderon, Atlas proposal 1660x, 2016.

364 [19] D. Santiago-Gonzalez, K. Auranen, M. Avila,
365 A. Ayangeakaa, B. Back, S. Bottoni, M. P. Carpen-
366 ter, J. Chen, C. M. Deibel, A. A. Hood, C. R. Hoff-
367 man, R. V. F. Janssens, C. L. Jiang, B. P. Kay,
368 S. Kuvin, A. Lauer, J. Schiffer, J. Sethi, R. Tal-
369 war, S. Zhu, *Probing the single-particle character*
370 *of rotational states in ¹⁹F using a short-lived iso-*
371 *meric beam*, arXiv:1801.02667 [nucl-ex].

372 URL <https://arxiv.org/abs/1801.02667>